RESEARCH ARTICLE | MAY 22 2023

Molten salt synthesis of $SrBi_{4-x}La_xTi_4O_{15}$ (X = 0.05, 0.10, 0.15, and 0.20) for Rhodamine-B degradation

Fikri Haikal; Anton Prasetyo

AIP Conference Proceedings 2580, 050005 (2023)
https://doi.org/10.1063/5.0122344

Molten Salt Synthesis of $SrBi_{4-x}La_xTi_4O_{15}$ (x = 0.05, 0.10, 0.15, and 0.20) for Rhodamine-B Degradation

Fikri Haikal and Anton Prasetyo [a)]

Department of Chemistry, Faculty Science and Technology, Universitas Islam Negeri Maulana Malik Ibrahim Malang, Jalan Gajayana No. 50 Malang, 65144, Indonesia

[a)] Corresponding author: anton@kim.uin-malang.ac.id

Abstract. – Four layered member Aurivillius compound $SrBi_4Ti_4O_{15}$ has been reported for its potential as a photocatalyst despite its weakness, such as the high recombination rate of electron-hole pair. Doped with rare earth elements such as lanthanum could solve the weakness. In this research, $SrBi_{4-x}La_xTi_4O_{15}$ (x = 0.05, 0.10, 0.15, and 0.20) were synthesized using molten salt flux Na_2SO_4/K_2SO_4 and evaluated the photocatalytic activity in rhodamine-B degradation. The diffractogram sample indicates that target materials were successfully obtained, although $SrTiO_3$ phase impurities were formed. The $SrBi_{4-x}La_xTi_4O_{15}$ (x = 0.05, 0.10, 0.15, and 0.20) particles exhibit plate-like morphologies with agglomerates. Band-gap energy was calculated using the Kubelka-Munk equation from the UV-Vis DRS spectrum, and we obtained that its band-gap energy ranges from 3.02-2.97 eV. Sample containing the highest Lanthanum content (x=0.20) exhibit the best rhodamine-b degradation with 26.27% degraded after 60 minutes reaction under UV-light irradiation.

BACKGROUND

High photocatalytic activity has been reported for Aurivillius phase ferroelectric materials such as Bi_2MO_6, $Bi_4Ti_3O_{12}$, and $Bi_5Ti_3FeO_{15}$ [1-3]. These properties have been attracted many researchers to investigate their application, for example, to degrade dye-waste pollution [1-3]. Aurivillius phase ($A_{m-1}B_mBi_2O_{3m+3}$) arranged from both the pseudo perovskite and bismuth layer alternately. Cation-*A* has large ionic radii, i.e., Bi, La, Nd, Sr, and Ba, while cation-*B* has small ionic radii, i.e., Ti, Fe, Co, and Ni; meanwhile, the number of the pseudo-perovskite layer can be identified by the *m* value[4].

Four layered member Aurivillius phase $SrBi_4Ti_4O_{15}$ exhibit excellent photocatalyst properties with band-gap energy ranged from 2.93-3.01 eV [5, 6]. It reveals an excellent opportunity for its utilization as a photocatalyst as it could work under visible light irradiation. The previous report showed the promising activities from $SrBi_4Ti_4O_{15}$ as a photocatalyst to degrade methyl orange solution [5]. On the other hand, some improvement could be implemented to $SrBi_4Ti_4O_{15}$ as it has a relatively high rate of electron and hole photorecombination activities [6].

Band-gap energy and recombination electron-hole rate are influencing the photocatalyst material performance. Ideally, photocatalyst should have a relatively low band-gap energy and low recombination electron-hole rate [7, 8]. One of many strategies to overcome this threat is to dope rare-earth elements into photocatalyst compounds [7-10]. Lanthanum can be used as a dopant in Aurivillius phase materials and was reported to successfully promote $Bi_5Ti_3FeO_{15}$'s photocatalytic activities to degrade the rhodamine-b solution [1]. Particle morphology also was reported to influences the photocatalytic activity of a material. Particles with large surface area and uniform size could enhance electron and hole pair migration, making separation effective, lowering the photorecombination rate [11]. Therefore, in this research, $SrBi_{4-x}La_xTi_4O_{15}$ (x = 0.05, 0.10, 0.15, and 0.20) has been synthesized using molten salt Na_2SO_4/K_2SO_4 flux then tested for its activity to degrade rhodamine-b dye solution.

Engineering Physics International Conference 2021 – EPIC 2021
AIP Conf. Proc. 2580, 050005-1–050005-6; https://doi.org/10.1063/5.0122344
Published by AIP Publishing. 978-0-7354-4484-3/$30.00

METHODOLOGY

Material

Materials used in this research are Bi_2O_3 (Himedia, 99,9% powder), $SrCO_3$ (Sigma-Aldrich, 99,9% powder), TiO_2 (Sigma-Aldrich, 99% powder), La_2O_3 (Sigma-Aldrich, 99% powder), Na_2SO_4 (99,5% Merck, powder), K_2SO_4 (Merck, powder), $AgNO_3$, aquadest and acetone.

$SrBi_{4-x}La_xTi_4O_{15}$ (x = 0.05, 0.10, 0.15 & 0.20) Synthesis

$SrBi4_{-x}La_xTi_4O_{15}$ (x = 0.05, 0.10, 0.15 & 0.20) synthesized using molten salt Na_2SO_4/K_2SO_4 flux method [12]. 2.5 gr target samples were produced by grinding $SrCO_3$, Bi_2O_3, TiO_2, La_2O_3, Na_2SO_4, dan K_2SO_4 with calculated stoichiometric composition for 60 minutes. Acetone is added accordingly to help the homogenization process evenly. After the mixture was evenly mixed, it was put into an alumina crucible and was heated for 750-850°C for 6 hours. The solids from the alumina crucible were washed by aqua dest until they were clean from both Na_2SO_4 and K_2SO_4 salts. The filtered powder then dried up in the oven at 750-850°C for 3 hours straight.

Material Characterization

The samples obtained were characterized using X-Ray Diffraction (XRD) technique (Rigaku Miniflex diffractometer; Cu $K\alpha$ (λ = 1,540593 Å)). The measurement used 2θ (°) ranged from 3-90°. Diffractogram data was refined by the Rietveld refinement method to acquire their crystallographic data using Multiphase Rietveld refinement on FullProf Suite (September 2020 Version). Particle morphology was examined by scanning electron microscope-energy (SEM) (Jeol JSM-6510). The optical properties were measured using ultraviolet-visible diffuse reflectance spectroscopy (UV-Vis DRS) (Thermo Scientific Evolution 220 spectrometer) with 200–800 nm wavelengths. The collected spectrum was calculated using the Kubelka-Munk equation to obtain their band-gap energy.

Photocatalytic Activities Test

A series of photocatalytic activity tests were conducted using 100 mL rhodamine-b solution (8.10^{-6} M). 0.1 grams samples were added into solution then stirred using a magnetic stirrer for 30 minutes in a dark environment to acquire adsorption-desorption equilibrium. The test was carried on under UV light irradiation from 9 ultraviolet lamps (Gaxindo T5 N093 8 Watt) for 30 and 60 minutes reaction. Rhodamine-b solution concentration before and after the reaction was evaluated using UV-Vis Spectroscopy (Thermo Scientific Evolution 220 spectrometer) with λ_{max} = 553.4 nm.

RESULT AND DISCUSSION

The sample's diffractogram is shown in Fig. 1. $SrBi_{4-x}La_xTi_4O_{15}$ (x = 0.05, 0.10, 0.15, and 0.20) were successfully synthesized using the molten salts method according to the comparison between diffractogram sample and diffractogram standard of $SrBi_4Ti_4O_{15}$ in Inorganic Crystal Structure Database (ICSD) number 5186. The corresponding peaks for and ICSD-5186 were marked with black circles. The inset picture in Fig.1 showed a shifting peak on 2θ= 30.8° into a higher position for higher lanthanum content and indicated that crystal lattice size was shrinking as lanthanum content increases. However, the ionic radii (r) of La^{3+} into Bi^{3+} is somewhat similar [13]; therefore, it can be assumed that ionic radii size was not responsible for this result. A similar result was reported in previous research, and it was resulted from the absence of a lone-pair electron in La^{3+} ion compared to replaced Bi^{3+} ion [1]. $SrTiO_3$ phase was found as an impurity, detected from 2θ= 32,4° peak on all samples. Difficulties on single-phase synthesis of lanthanum doped $SrBi_4Ti_4O_{15}$ was caused by instability resulted from higher lanthanum concentration doping since it can replace Bi^{3+}-sites on the bismuth layer [1, 14, 15].

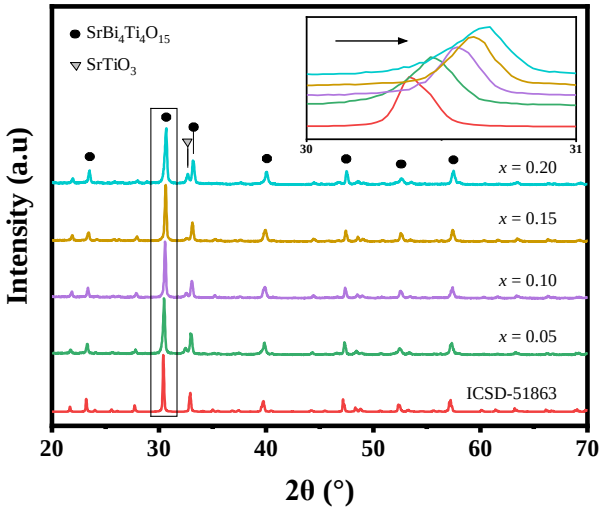

FIGURE 1. XRD Diffractogram of $SrBi_{4-x}La_xTi_4O_{15}$ (x = 0.05, 0.10, 0.15, and 0.20)

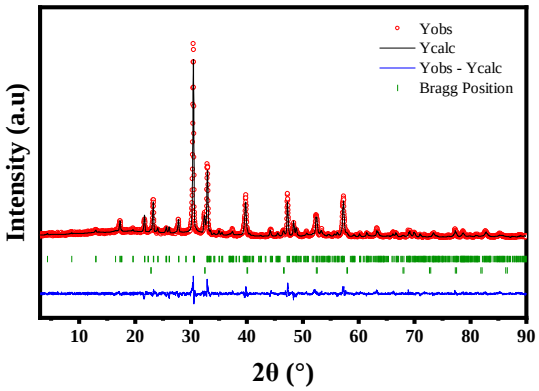

FIGURE 2. Diffractogram Multiphase refinement of $SrBi_{4-x}La_xTi_4O_{15}$ (x = 0.05)

Crystallographic data for $SrBi_{4-x}La_xTi_4O_{15}$ (x = 0.05, 0.10, 0.15 & 0.20) summarized on Table 1 resulted from multiphase Rietveld refinement from their diffractograms using ICSD-No. 51863 standard for $SrBi_4Ti_4O_{15}$ with $A2_1am$ space group and ICSD-No. 91899 standard for $SrTiO_3$ with $Pm\text{-}3m$ space group. The refinement plot of $SrBi_{4-x}La_xTi_4O_{15}$ (x = 0.05) was showed in Fig 2. R_{wp} value can be the determining factor for a 'good' refinement, the lower, the better. x= 0.20 has the highest R_{wp} values of 28.5%. Despite its high R_{wp} value, our refinement is good if we look closely at Figure 2; in refinement, we had to look at the number and the quality of our data [16]. Noise or background in the data can be attributed to high agreement between calculated and experimental data, hence lower R_{wp} value [16]. All of our refinement is good enough with R_{wp} value ranged from 20-30%, and has a relatively flat blue line (sample-standard fitness).

Multiphase refinement could estimate the percentage of each phase on our sample. From Table 1, we knew that $SrTiO_3$ formed in our samples was decreasing from x= 0.05-0.15 and increases for x= 0.20. Substitution of La^{3+} ion into Bi^{3+} sites on the perovskite layer responsible for x= 0.05-0.15 and resulted in decreased orthorhombic distortion in the crystal lattice because of the lack of lone-pair electron. On the other hand, the x= 0.20 replaced Bi3+ on the bismuth layer, causing structure instability; thus, higher $SrTiO_3$ was formed [15, 17].

TABLE 1. The Crystallography data of $SrBi_{4-x}La_xTi_4O_{15}$ (x= 0.05, 0.10, 0.15, and 0,20)

Parameter	$SrBi_{4-x}La_xTi_4O_{15}$			
	x= 0.05	x= 0.10	x= 0.15	x= 0.20
Crystal lattice	Orthorombic	Orthorombic	Orthorombic	Orthorombic
Space group	$A2_1am$	$A2_1am$	$A2_1am$	$A2_1am$
a (Å)	5.4388	5.4508	5.4482	5.4365
b (Å)	5.4268	5.4347	5.4357	5.4327
c (Å)	40.9751	40.9800	40.9844	41.0383
Cell volume (Å^3)	1209.4032	1213.9668	1213.7307	1212.0610
R_p (%)	24.6	21.9	21.8	28.4
R_{wp} (%)	24.4	22.3	22.6	28.5
R_{exp} (%)	7.65	7.37	7.20	7.74
GoF (χ^2)	10.15	9.149	9.869	13.58
% $SrTiO_3$	16.94	15.25	7.32	22.50

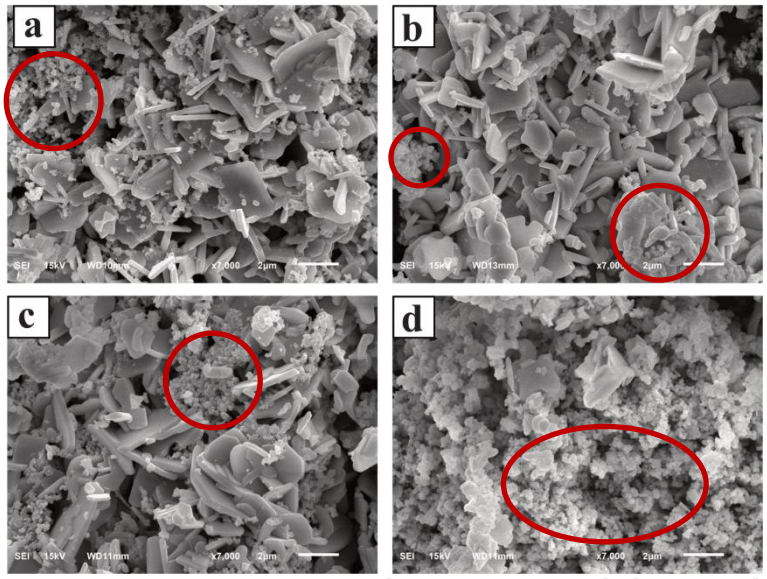

FIGURE 3. Micrograph of $SrBi_{4-x}La_xTi_4O_{15}$ (x= (a) 0.05, (b) 0.10, (c) 0.15, and (d) 0.20) (red circle mark denotes the agglomeration)

$SrBi_{4-x}La_xTi_4O_{15}$ (x= 0.05, 0.10, 0.15, and 0.20) particles morphologies were depicted on Fig 3. It can be seen that platelike particles were formed. Many researchers reported that the platelike particle is characteristic of Aurivillius phase materials [18]. SEM images also present the form of the agglomerated particle in our samples (red circle mark). The formed agglomerates were a consequence of $SrTiO_3$ impurities found in all samples [19-21].

Tauc plotting from UV-Vis DRS and the calculated band-gap energy each showed in Fig 4 and summarized in Table 2. The Band-gap energy value attained by $SrBi_{4-x}La_xTi_4O_{15}$ (x= 0.05, 0.10, 0.15, and 0.20) were incrementally smaller from $SrBi_4Ti_4O_{15}$ (E_g= 3.00 eV) [6]. This suggests that doping can decrease the band-gap energy of Aurivillius phase material. Band-gap energy decrease was subjected to a phenomenon called quantum confinement for smaller size particles caused by La^{3+} ion doping [22, 23]. Another report suggested that lanthanum doping caused Ti-O electron density change along with increases in A-site steric strain [24]. Previous research also found that lanthanum doping in Aurivillius phase material acts as a capturer of the electron produced in the excited state of photocatalyst, resulting in a lower recombination rate between the electron and hole essentials for the photocatalytic reaction [8]. Unfortunately, it was not investigated in our research because of impurities found in our sample.

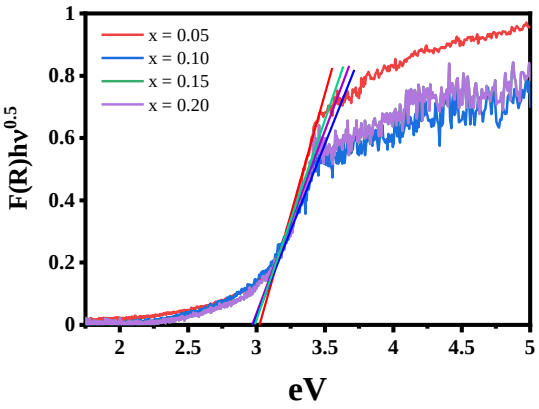

FIGURE 4. Tauc Plotting of $SrBi_{4-x}La_xTi_4O_{15}$ (x= 0.05, 0.10, 0.15, and 0,20)

TABLE 2. $SrBi_{4-x}La_xTi_4O_{15}$ (x= 0.05, 0.10, 0.15, and 0,20) band-gap energy

$SrBi_4Ti_{4-x}La_xO_{15}$	Band-gap energy (eV)	Wavelength (nm)
x = 0,05	3.02	410.54
x = 0.10	2.98	416.05
x = 0.15	2.99	414.66
x = 0.20	2.97	417.46

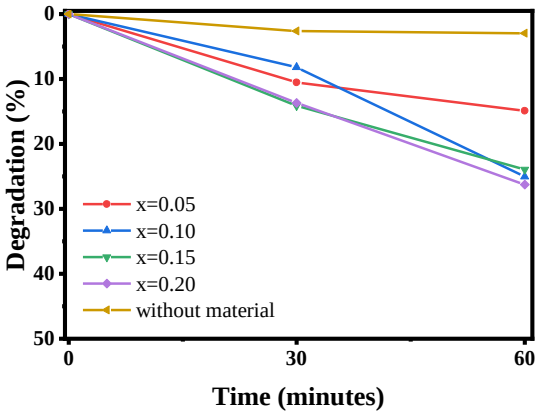

FIGURE 5. Photocatalytic Degradation of Rhodamine-B by $SrBi_{4-x}La_xTi_4O_{15}$ (x= 0.05, 0.10, 0.15, and 0.20)

Photocatalytic activities for $SrBi_{4-x}La_xTi_4O_{15}$ (x= 0.05, 0.10, 0.15, and 0.20) was evaluated in degrading rhodamine-b solution, and the result showed on Figure 5. Sample with La^{3+} content 0.20 (x= 0.20) had the highest photocatalytic activities degrading 26.27% of rhodamine-b solution within 60 minutes reaction under UV-light irradiation. Enhancement in photocatalytic activity of our samples generated by smaller platelike particles formed as lanthanum-ion increases [25]. From the optical perspective, band-gap energy is close to negligible since it does not show a significant difference between those four samples. Meanwhile, the role of recombination electron-hole to activity photocatalytic did not investigate in this research.

CONCLUSION

La^{3+} ion doping increased on Aurivillius phase $SrBi_{4-x}La_xTi_4O_{15}$ (x= 0.05, 0.10, 0.15, and 0.20) could increase their photocatalytic activities on degrading rhodamine-b dye solution. Particles with platelike morphology were found in

all samples and encountered size shrinking as La^{3+} increases. Even though the band-gap energy was not significantly reduced, the $x = 0.20$ sample was successfully degraded 26.27% rhodamine-b solution within 60 minutes of reaction under UV-light irradiation.

REFERENCES

1. G. Naresh and T. K. Mandal, ACS Appl Mater Interfaces **6** (23), 21000-21010 (2014).
2. X. Liu, S. Gu, Y. Zhao, G. Zhou, and W. Li, J Mater Sci Technol **56**, 45-68 (2020).
3. S. Niu, R. Zhang, X. Zhang, J. Xiang, and C. Guo, Ceram. Int. **46** (5), 6782-6786 (2020).
4. X. Xie, H. Sun, Z. Xu, M. Wang, X. Chen, and J. Han, New J. Chem. **43** (37), 14714-14719 (2019).
5. H. Xie, K. Wang, Y. Yao, Y. Zhao, and X. Wang, AMC **01** (01), 1-4 (2013).
6. P. Nayak, T. Badapanda, R. Pattanayak, A. Mishra, S. Anwar, P. Sahoo, and S. Panigrahi, Metal and Mat Trans A **45** (4), 2132-2141 (2014).
7. A. A. Alemi, R. Kashfi, and B. Shabani, J Mol Catal A-Chem **392**, 290-298 (2014).
8. D. Wang, H. Shen, L. Guo, C. Wang, F. Fu, and Y. Liang, RSC Advances **6** (75), 71052-71060 (2016).
9. Z. Dai, F. Qin, H. Zhao, J. Ding, Y. Liu, and R. Chen, ACS Catalysis **6** (5), 3180-3192 (2016).
10. X. Zhang, H. Zhang, H. Jiang, F. Yu, and Z. Shang, Catal Letters **150** (1), 159-169 (2020).
11. R. He, D. Xu, B. Cheng, J. Yu, and W. Ho, Nanoscale Horiz **3** (5), 464-504 (2018).
12. Zulhadjri, S. E. Afni, and S. Arief, Prosiding Semirata FMIPA Universitas Lampung **6** (2013), 489-494.
13. R. Shannon, Acta Crystallogr., Sect. A: Found. Crystallogr. **32** (5), 751-767 (1976).
14. R. Z. Hou and X. M. Chen, Solid State Commun. **130** (7), 469-472 (2004).
15. P. Nayak, T. Badapanda, and S. Panigrahi, J Mater Sci: Mater Electron **28** (1), 625-632 (2017).
16. B. H. Toby, Powder Diffr. **21** (1), 67-70 (2006).
17. J. Zhu, J.-H. He, and X.B. Chen, Integr. Ferroelectr. **79** (1), 265-271 (2006).
18. A. Faraz, J. Ricote, R. Jimenez, T. Maity, M. Schmidt, N. Deepak, S. Roy, M. E. Pemble, and L. Keeney, Int. J. Appl. Phys. **123** (12), 124101 (2018).
19. Q.-Y. Tang, Y.-M. Kan, P.-L. Wang, Y.-G. Li, and G.-J. Zhang, J. Am. Ceram. Soc. **90** (10), 3353-3356 (2007).
20. A. Kikuchihara, F. Sakurai, and T. Kimura, J. Am. Ceram. Soc. **95** (5), 1556-1562 (2012).
21. T. Kimura, in *Advances in Ceramics - Synthesis and Characterization, Processing and Specific Applications*, edited by C. Sikalidis (IntechOpen, IntechOpen, 2011).
22. R. E. Marotti, P. Giorgi, G. Machado, and E. A. Dalchiele, Sol. Energy Mater Sol. Cells **90** (15), 2356-2361 (2006).
23. P. Zhang, Y. Yi, C. Yu, W. Li, P. Liao, R. Tian, M. Zhou, Y. Zhou, B. Li, M. Fan, and L. Dong, J Mater Sci: Mater Electron **29** (10), 8617-8629 (2018).
24. S. G. Hur, T. W. Kim, S.J. Hwang, and J. H. Choy, J. Photochem. Photobiol. **183** (1), 176-181 (2006).
25. W. Zhao, H. Wang, X. Feng, W. Jiang, D. Zhao, and J. Li, Mater. Res. Bull. **70**, 179-183 (2015).